

# Seismic events associated with catastrophic fracture propagation in rock under compression

Hongyu Wang, Arcady Dyskin,  
Elena Pasternak, Phil Dight

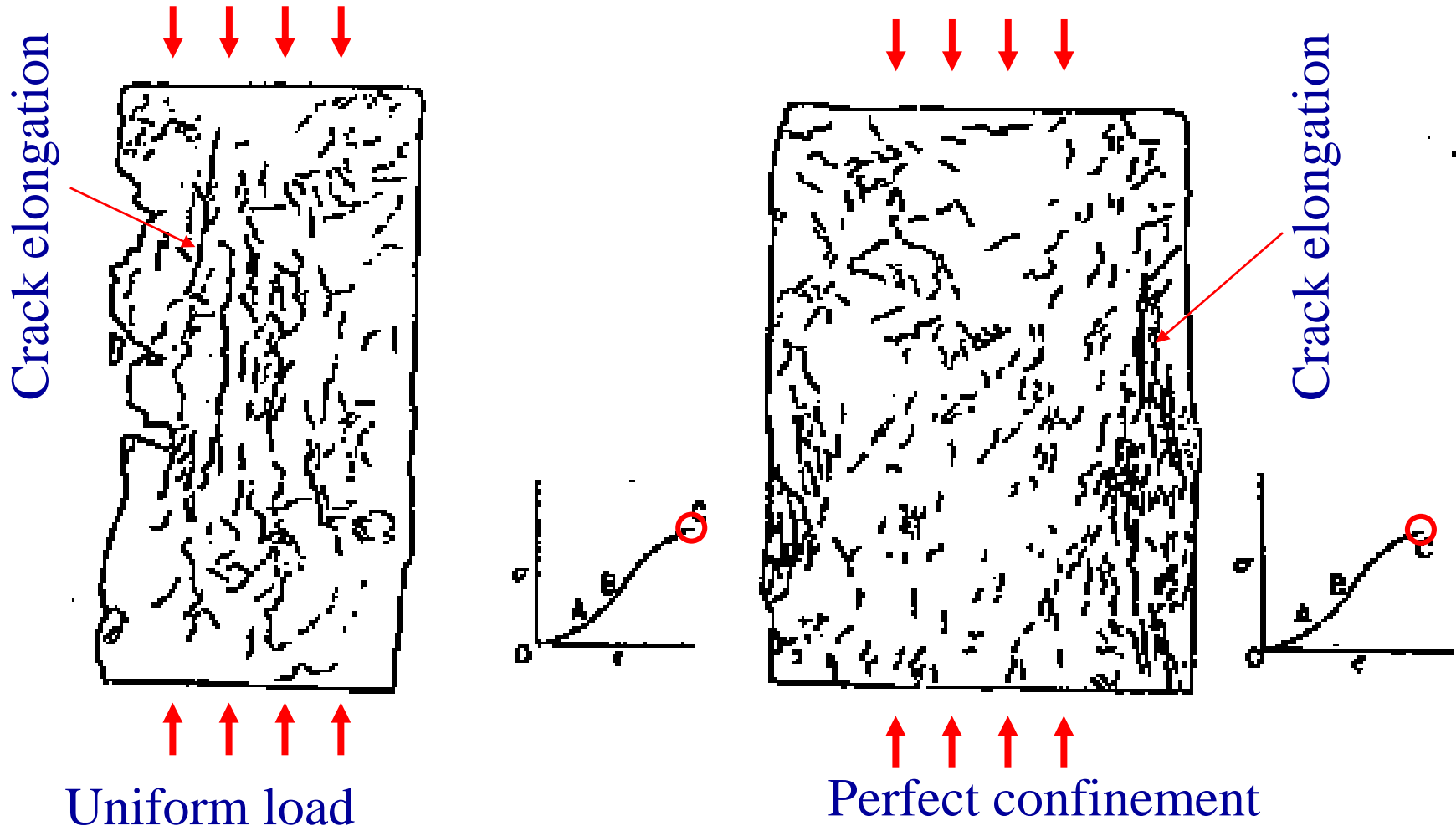
# Motivation

- Catastrophic crack propagation parallel to a free surface (e.g., excavation wall) is a mechanism that can cause a dangerous event such as a strain rockburst.
- Catastrophic crack propagation is accompanied by (micro)seismicity and hence can be detected.
- 3 phases of crack growth in compression are identified and presented here. These are:
  1. Crack initiation as a wing crack
  2. Extensive wing crack growth (under the conditions identified in the presentation). The growth is stable (stress increase is required to increase the crack dimensions)
  3. Onset of unstable crack propagation due to the effect of the free surface

# Evidence of development of internal cracks in compression

- Rocks are heterogeneous materials, which contain various defects or weakness at all scales.
  1. On the small scale, these defects include grain boundaries, pores, and cracks.
  2. On the larger scale, they are joints, faults and bedding planes.
- In compression, these defects work as sources of the initiation and growth of the subsequent cracks. The crack growth is closely associated with macroscopic behaviour of the rock, i.e. contributes to the pronounced nonlinearity of the stress-strain behaviour.
- The following slide shows rock samples under uniaxial compression. According to the stress-strain curve, when the rock sample is near the final failure, the crack elongation can be identified.

# Evidence of development of internal cracks in compression

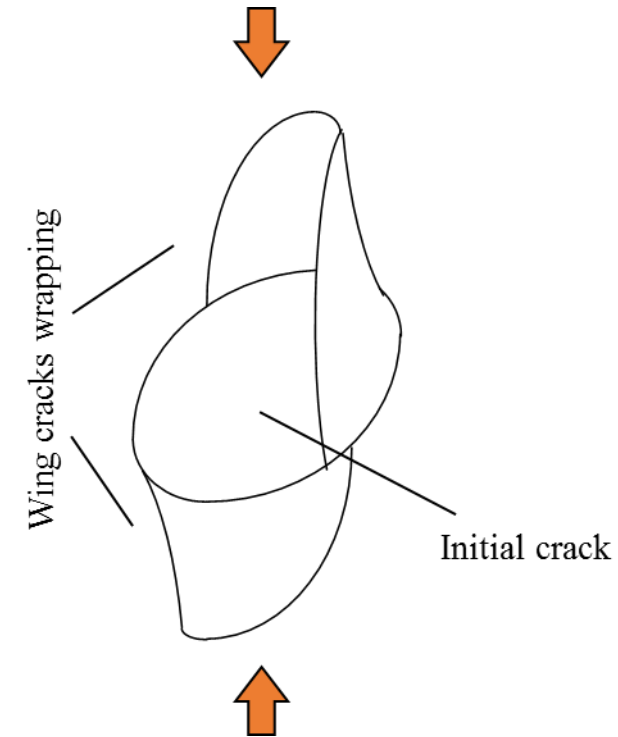
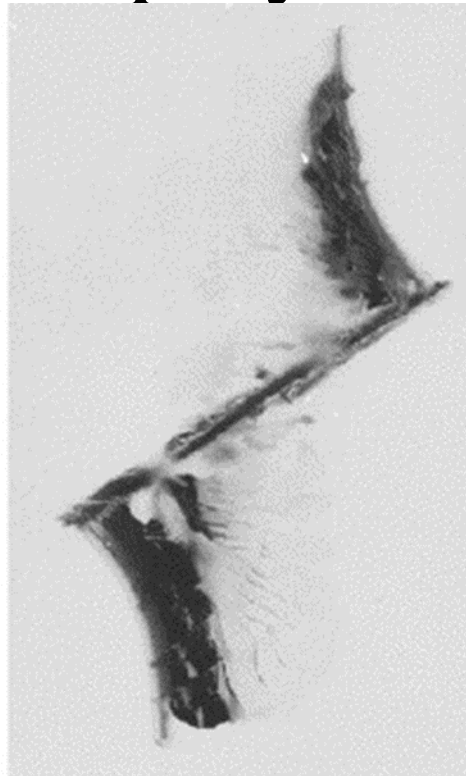
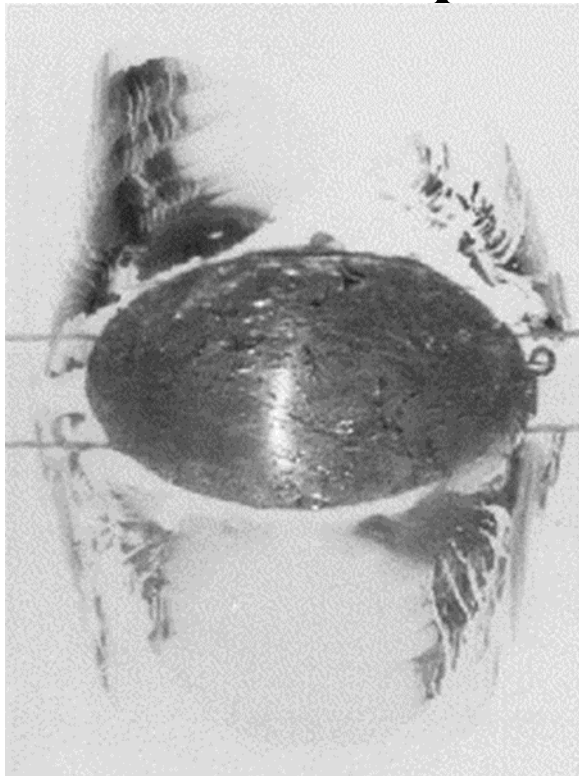


(after Peng & Johnson, 1972)

# 3-D crack growth in uniaxial compression, as observed in experiments with transparent polyester resin

- Previous direct experiments conducted show that in 3-D sample, the initial penny-shape crack located in the centre of the sample, the wing cracks are restricted to the sizes comparable to the initial crack and therefore cannot substantially grow to cause the macroscopic failure of the sample.
- The following slide shows the front view and the lateral view of the wing crack growth in a resin sample. The wings assume a special shape curving or wrapping around the initial crack. Subsequently this phenomenon is called wrapping.

# 3-D crack growth in uniaxial compression, as observed in experiments with transparent polyester resin



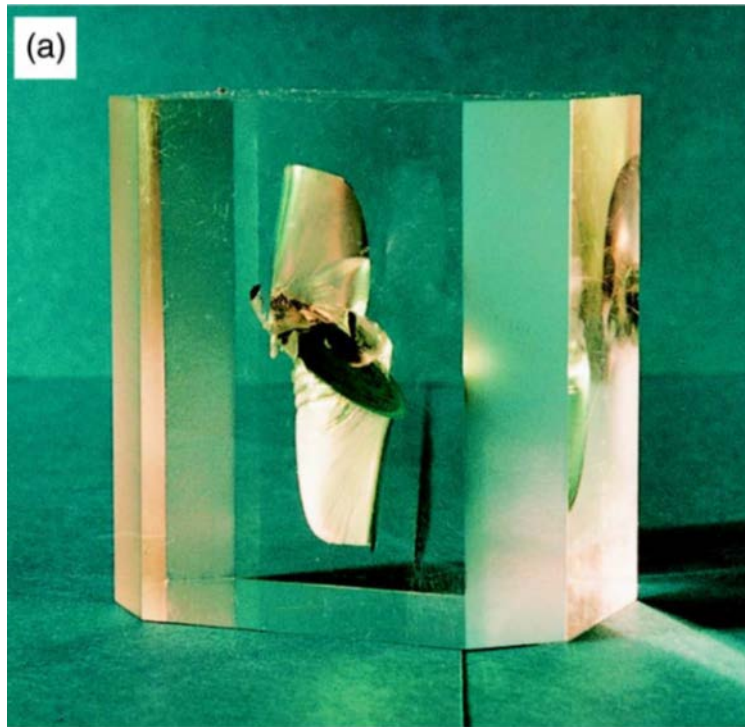
(after Dyskin et al, 2003, Wang et al, 2018)

**No extensive wing crack growth is possible**

# 3-D crack growth under uniaxial compression in other materials

- This wing crack wrapping was also verified to be consistent in samples made from various materials such as PMMA, glass, cement and mortar. In the following slide:
  1. Figure (a) shows wing crack growth in a PMMA sample, the initial crack is induced by laser. The size of upper and lower wings is comparable to the initial crack.
  2. In Figure (b), the remains of a cement sample with internal crack split in uniaxial compression is presented. It is seen that the splitting surface is perpendicular to the artificial crack. Thus, this splitting is caused by the failure by the cement material other than the crack growth, i.e. the crack growth is also limited.

# 3-D crack growth under uniaxial compression in other materials



PMMA sample

(after Germanovich and Dyskin et al, 2000)

28/04/2020



Cement sample

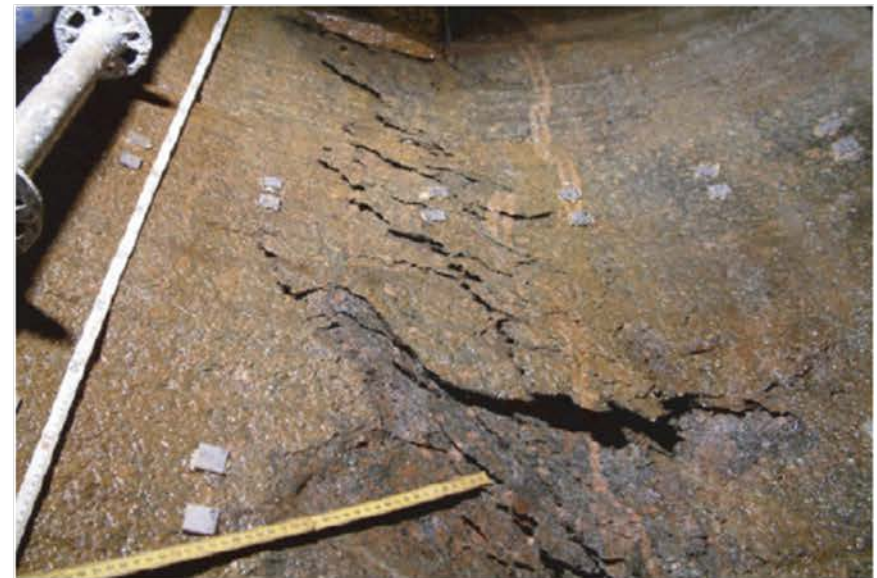
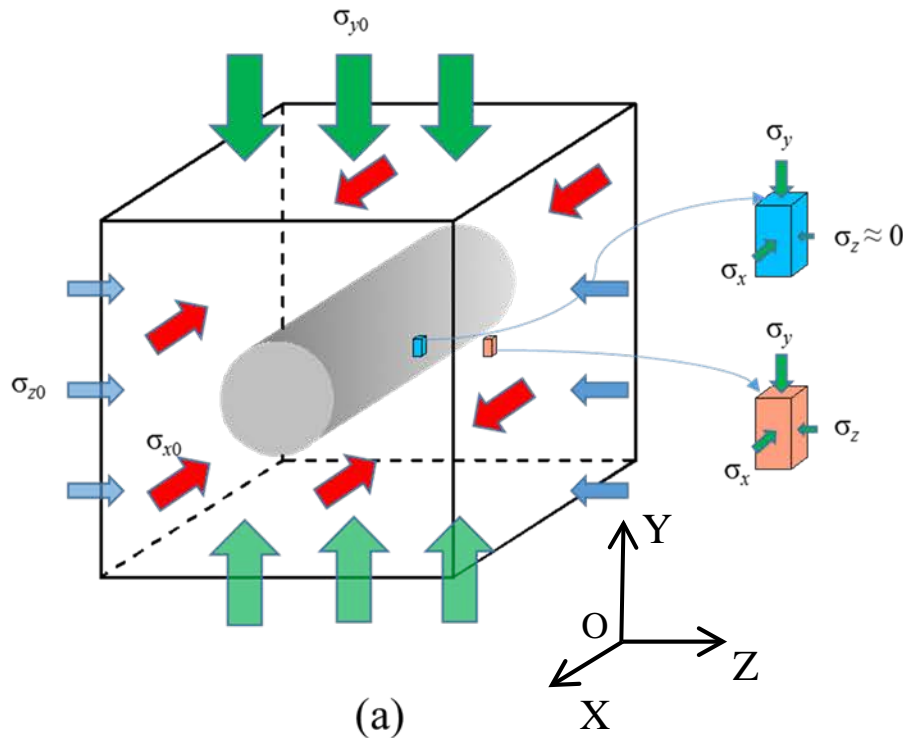
(after Dyskin et al, 2003)

Wang, A.V. Dyskin, Pasternak, Dight

# Stress regime in a rock mass with unsupported cylindrical excavation

- When excavating an opening, the stress in the rock elements at the excavation boundary increases in the tangential direction ( $y$ ) and reduces in the radial direction ( $z$ ). In the immediate vicinity of the (unsupported) excavation boundary (distances from the surface are small compared to the dimensions of the opening) the induced radial stress is almost zero ( $\sigma_z \approx 0$ ), figure (a) in the following slide.
- The stress (the intermediate principal stress  $\sigma_y$ ) along the excavation axis is always present. Therefore, the stress state of biaxial compression is formed.

# Stress regime in a rock mass with unsupported cylindrical excavation



An example of non-violent spalling fracture

(b)

# Strain rockburst at the sidewalls of an excavation

Surface  
parallel  
fractures

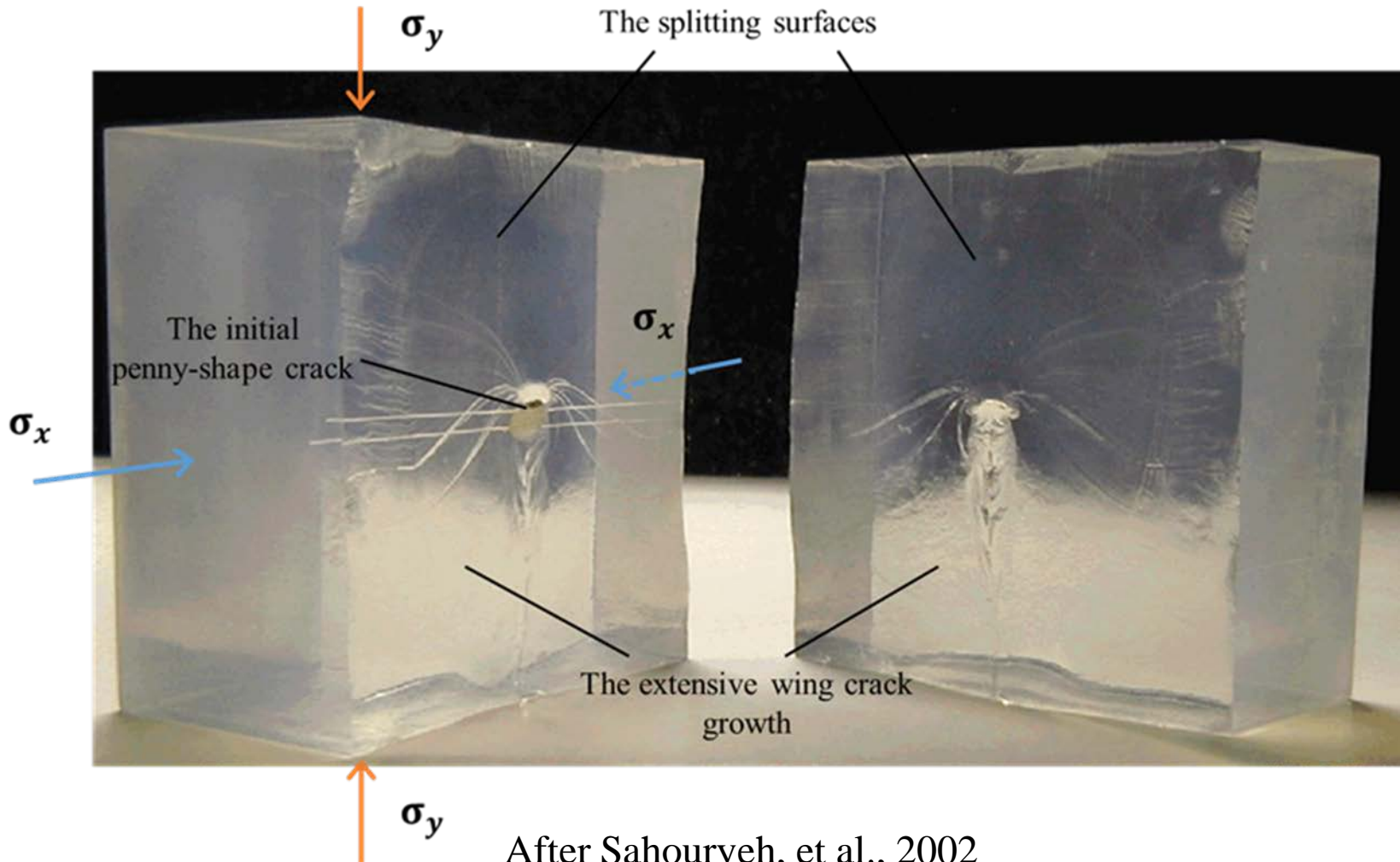


At a larger scale, a strainburst occurs.

# Extensive wing crack growth in biaxial compression

- It was found that the extensive crack growth can be induced in biaxial compression.
- Sahouryeh, et al. (2002) found that in biaxial compression with approximately equal loads (the biaxial load ratio  $\sim 1$ ), the pattern of growth of the initial crack dramatically differs from that observed in uniaxial compression. In biaxial compression, the second principal compressive stress prevents the overall wing cracks from wrapping, and therefore wing cracks were able to grow extensively parallel to both loading directions, which ultimately led to the splitting failure of the tested samples, as shown in the next slide.

# Extensive wing crack growth in biaxial compression

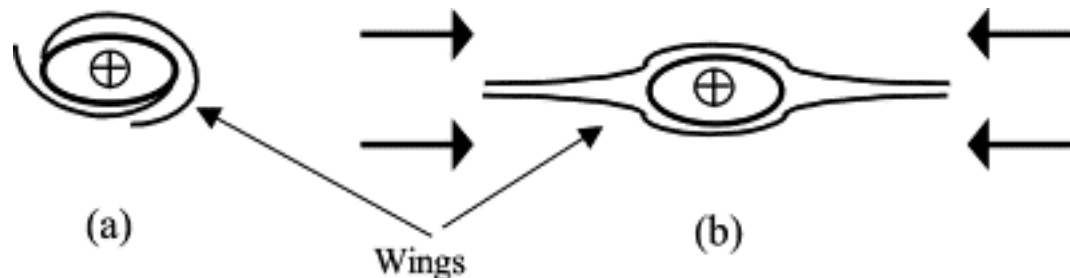


# Further experiments.

We now understand:

1. In uniaxial compression, the restricted wing crack is produced because of wing crack wrapping, figure (a).
2. In biaxial compression with the biaxial load ratio of 1, the extensive crack growth is produced, figure (b).

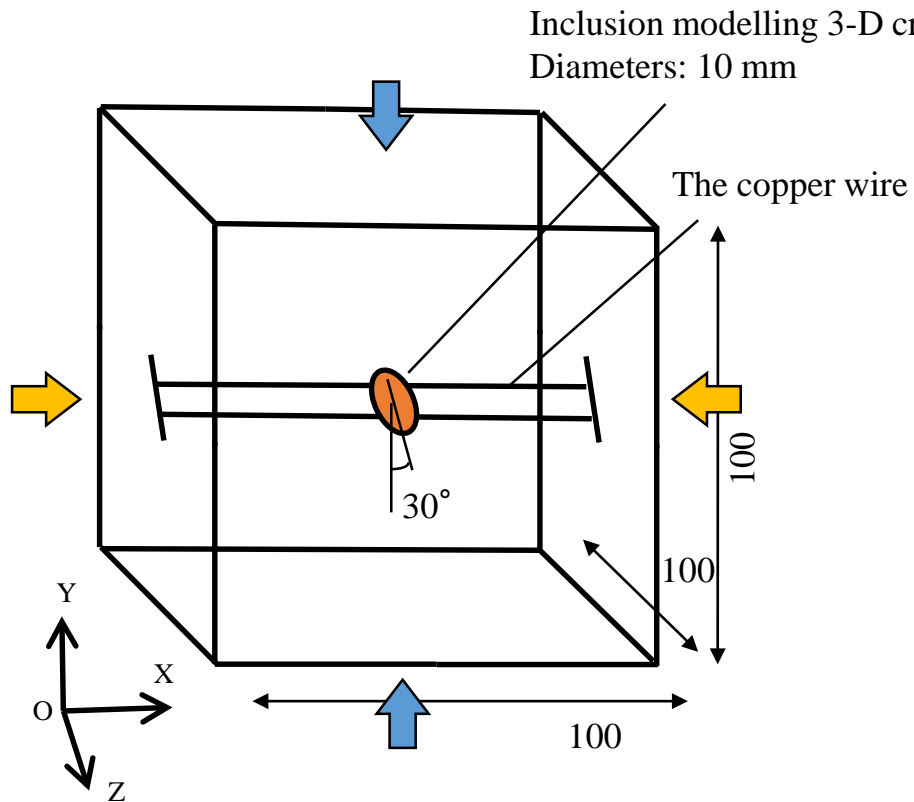
Therefore, it was important to explore the transition process between extensive and restricted crack growth pattern. Most importantly, the critical value of biaxial load ratio inducing the extensive crack growth needed to be determined.



# Resin sample preparation

- Cubic samples with the dimension of 100 mm were made from transparent casting polyester resin.
- To model the initial penny shape crack, two greased aluminium foil disks, 5 mm in radius, inclined at different angles to one of the loading axes (y-axis in the sketch) were hung in the centre of a cubic aluminium mould by a pair of copper wires prior to resin casting.
- Before pouring into the mould, the resin and the catalyst were mixed thoroughly to prevent the “strip-like” effect within samples.
- After being completely cured (around 7 days according to the resin casting manual), the samples were cut and polished to the required dimensions. The aluminium mould and a completed resin sample are shown in the next slide.

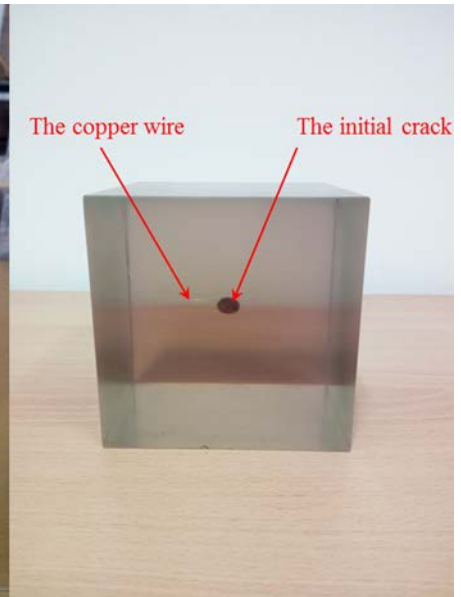
# Resin sample preparation



Sketch of the sample



Aluminium  
mould

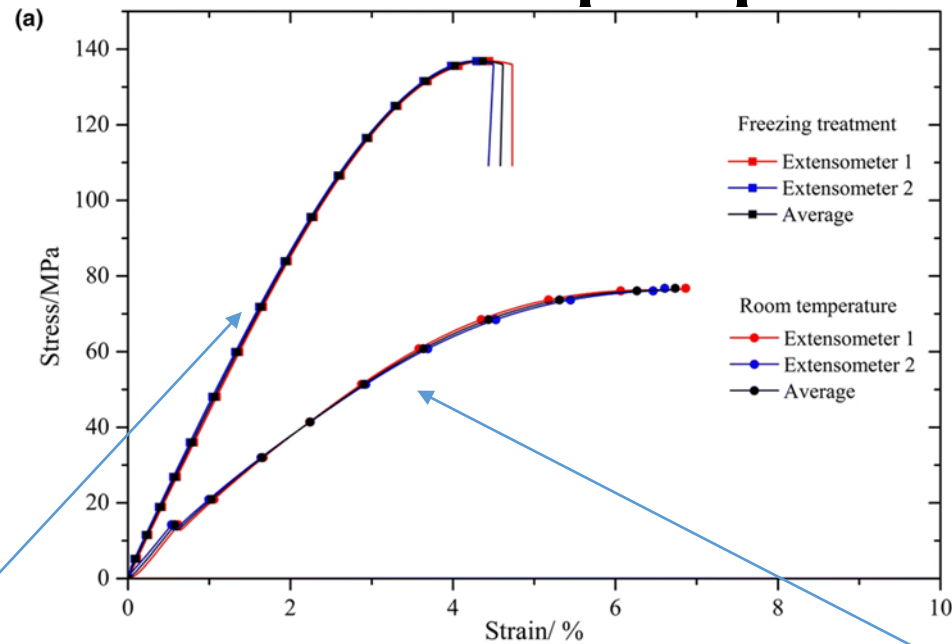


The completed  
sample

# The material properties

- To ensure a brittle failure regime, samples were kept in a freezer for at least 48 h (at  $\cong -16^{\circ}\text{C}$ ) before testing such that by the time of testing the temperature does not exceed the required  $-6^{\circ}\text{C}$ .
- The following slide shows the axial stress-strain curves (measured by two extensometers) of uniaxial compression tests on frozen resin sample with freezing treatment and of the sample kept in room temperature. It is seen that after freezing, the stress-strain curve corresponds to brittle material. Furthermore, the splitting failure mode is observed.

# The material properties



The stress-strain curves

Tested sample after freezing

(b)



Tested specimen with freezing treatment



Tested specimen at room temperature

Tested sample at room temperature

# True triaxial loading system



The loading platens applying  $\sigma_2$

The loading platens applying  $\sigma_2$

The resin sample      The loading platens applying  $\sigma_1$

# The experimental results

- The following slides present a typical testing results of the samples containing different types of the initial defects in biaxial compression with different biaxial load ratios ( $\sigma_x/\sigma_y$ ).

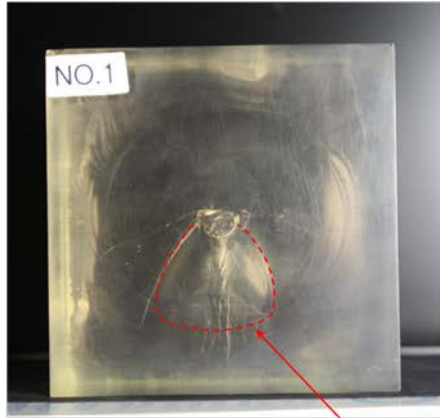
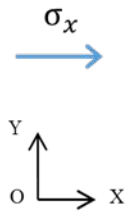
# The experimental results Penny-shape crack inclined at $30^\circ$ to $\sigma_y$

The biaxial load ratio

$$\sigma_x / \sigma_y = 0.5$$

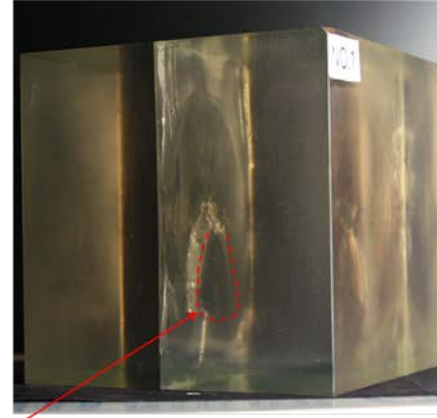
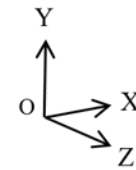


The front view



(a)

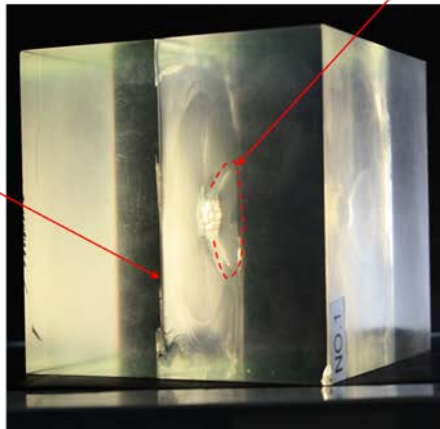
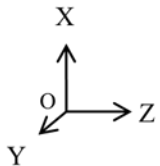
The lateral view



(b)

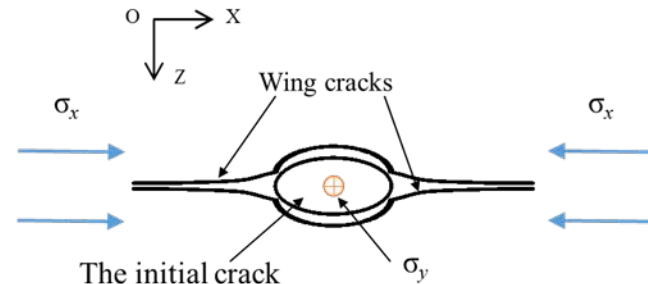
The top view

The extensive wing crack growth



(c)

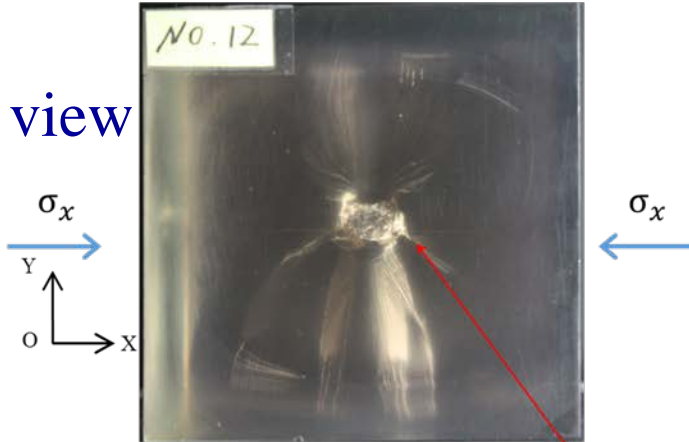
The "moth-shape" wing crack



(d)

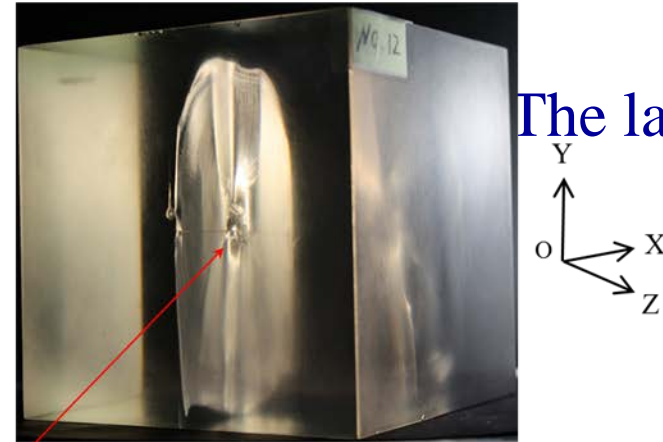
The biaxial load ratio  $\sigma_x/\sigma_y = 0.06$

The front view



(a)  $\sigma_y$

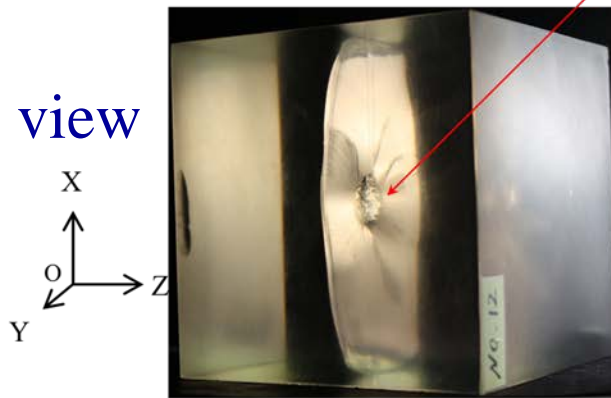
The lateral view



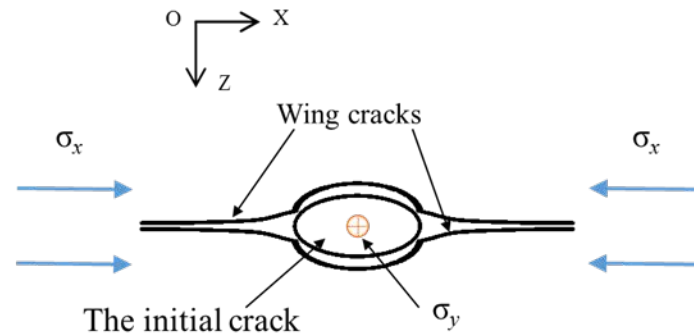
(b)

The wavy shape near the initial crack

The top view



(c)



(d)

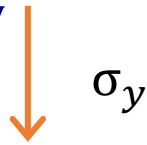
# The experimental results

Square-shape crack inclined at  $30^\circ$  to  $\sigma_y$

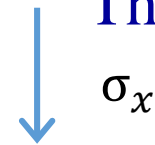
The biaxial load ratio

$$\sigma_x / \sigma_y = 0.5$$

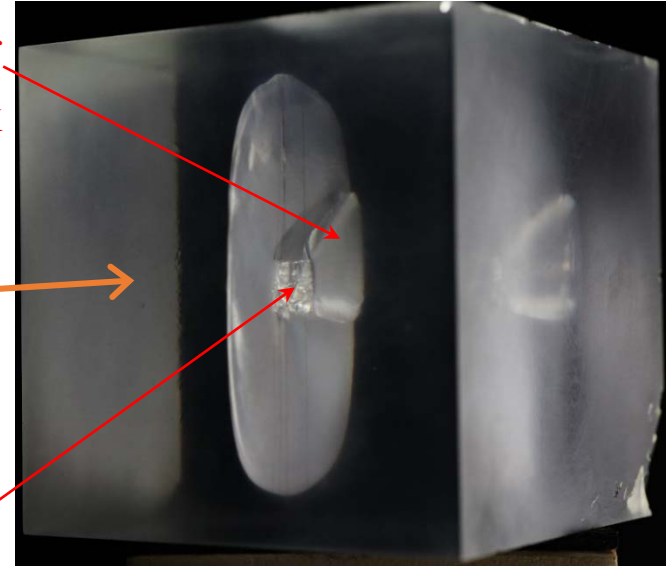
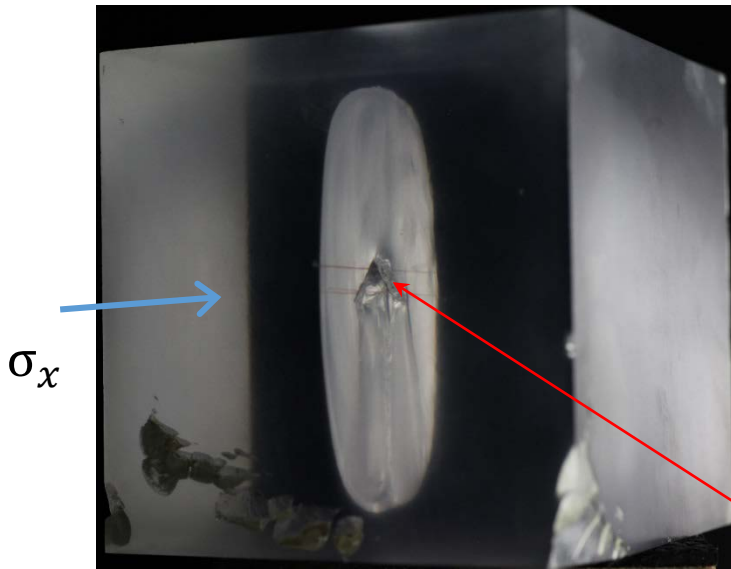
The lateral view



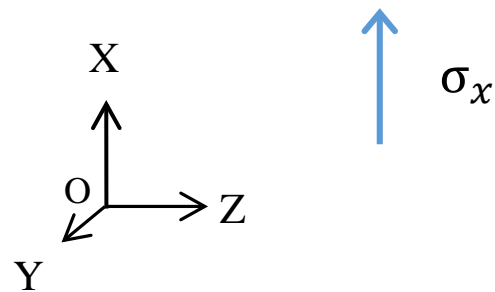
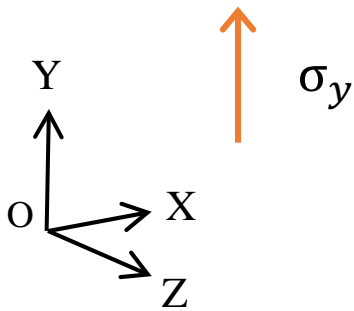
The top view



The wing crack sprouting from the lower tip of the initial crack



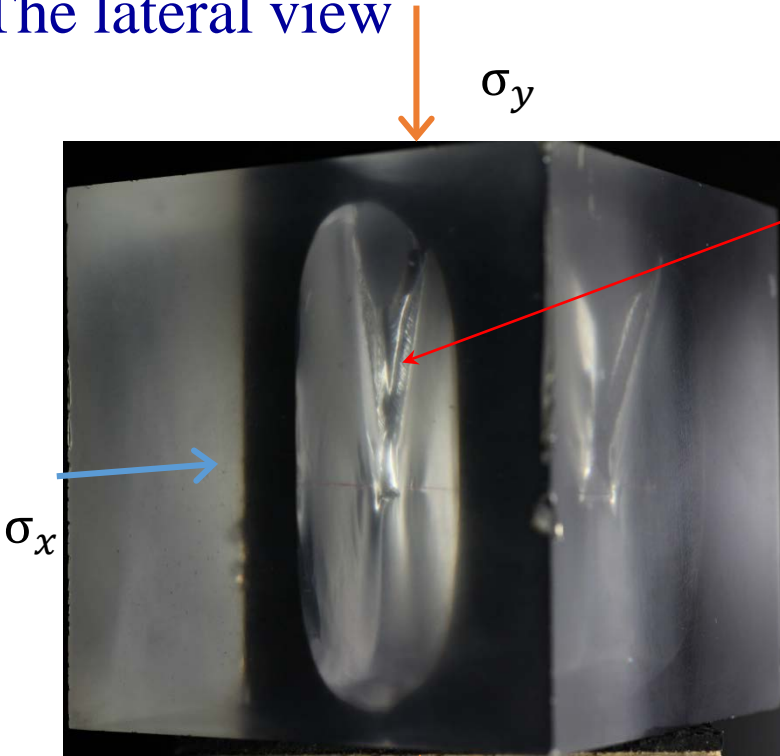
The initial square-shape crack



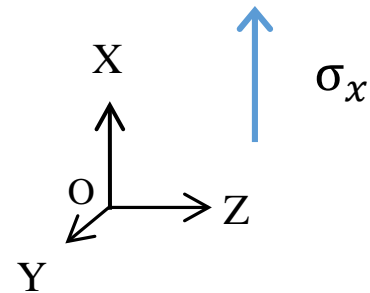
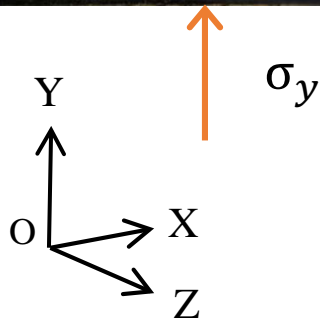
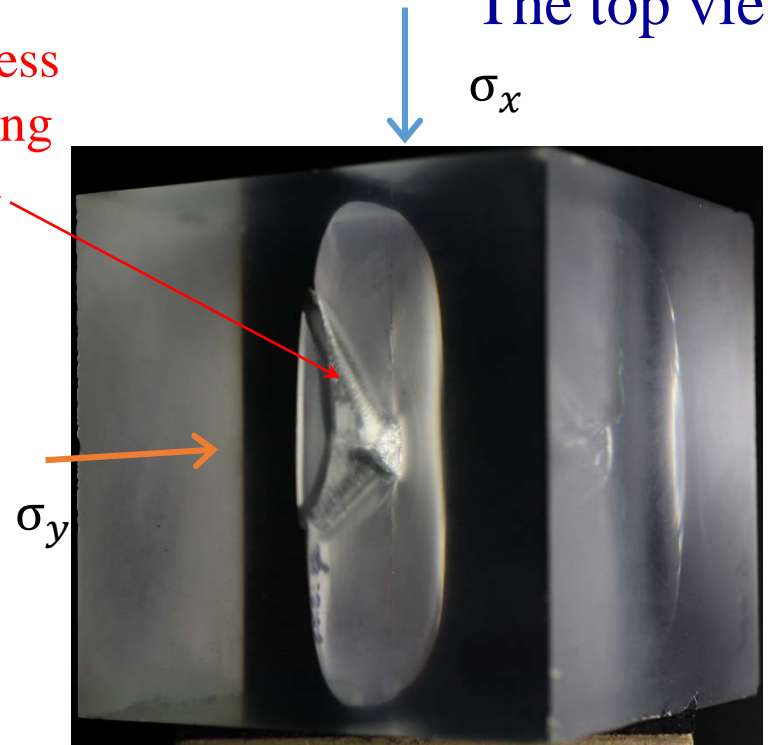
The biaxial load ratio  $\sigma_x/\sigma_y = 0.06$

The lateral view

The top view



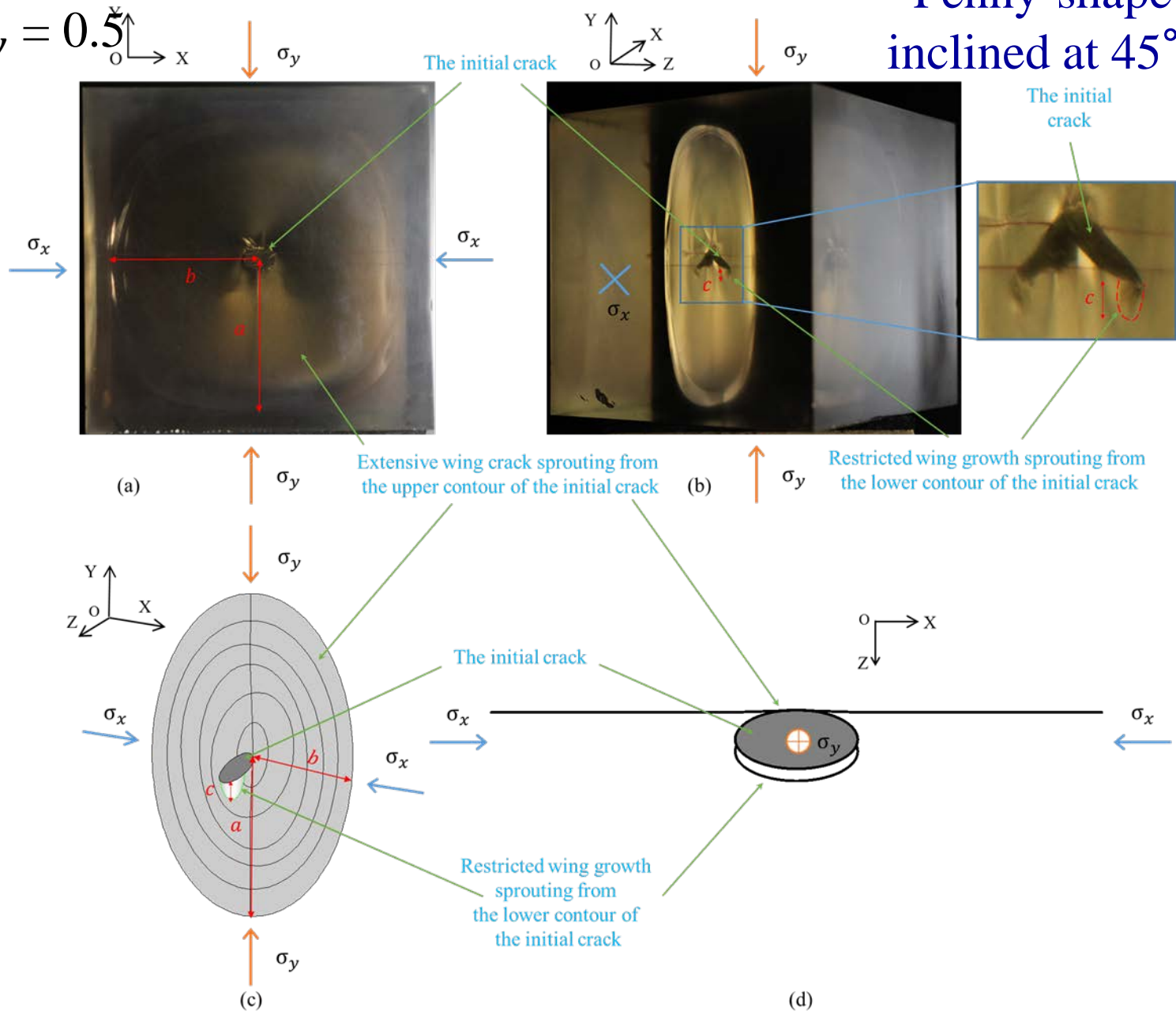
Discreteness  
of the wing  
surface



# The biaxial load ratio

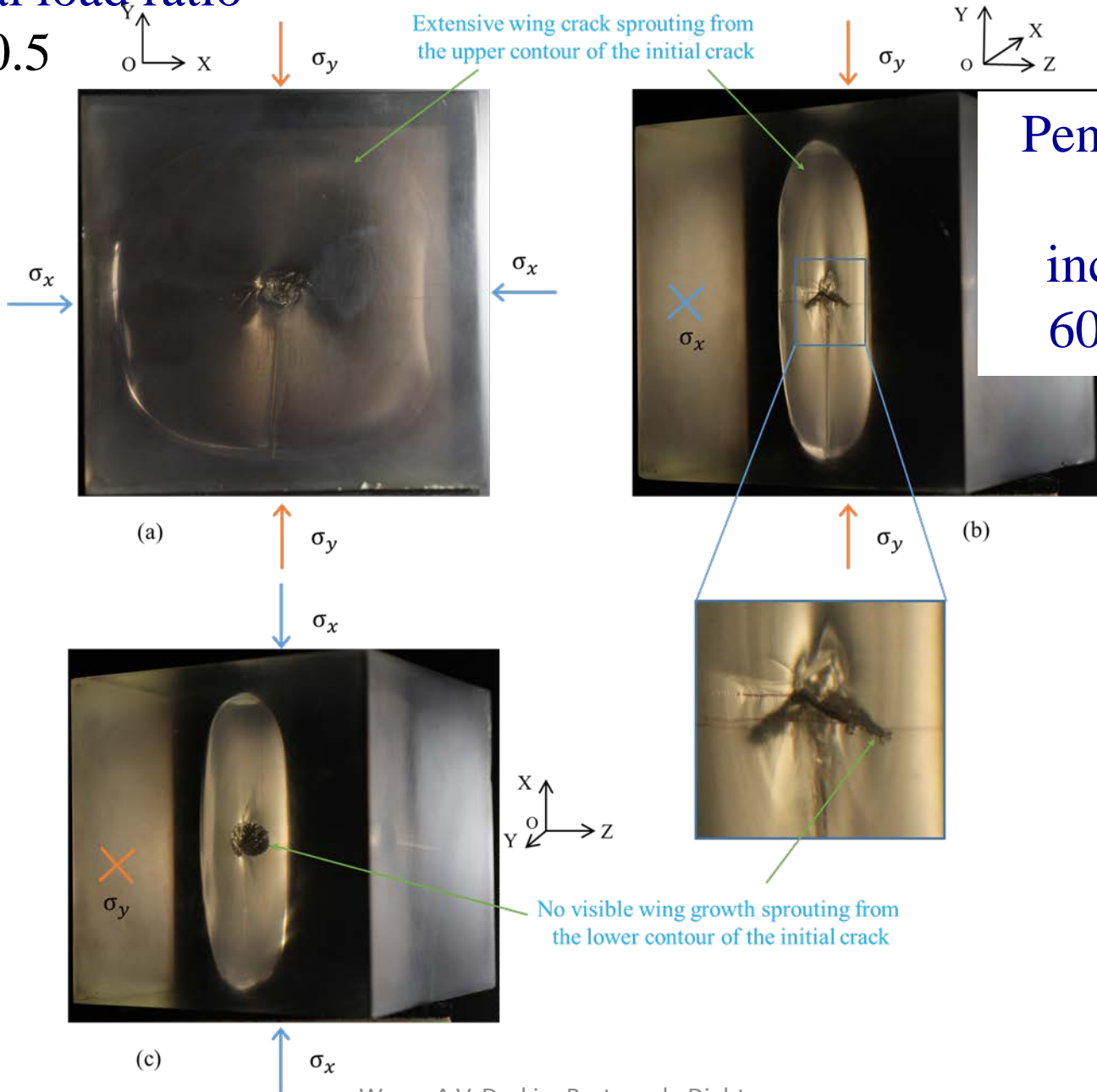
$$\sigma_x / \sigma_y = 0.5$$

# Penny-shape crack inclined at $45^\circ$ to $\sigma_y$



# The biaxial load ratio

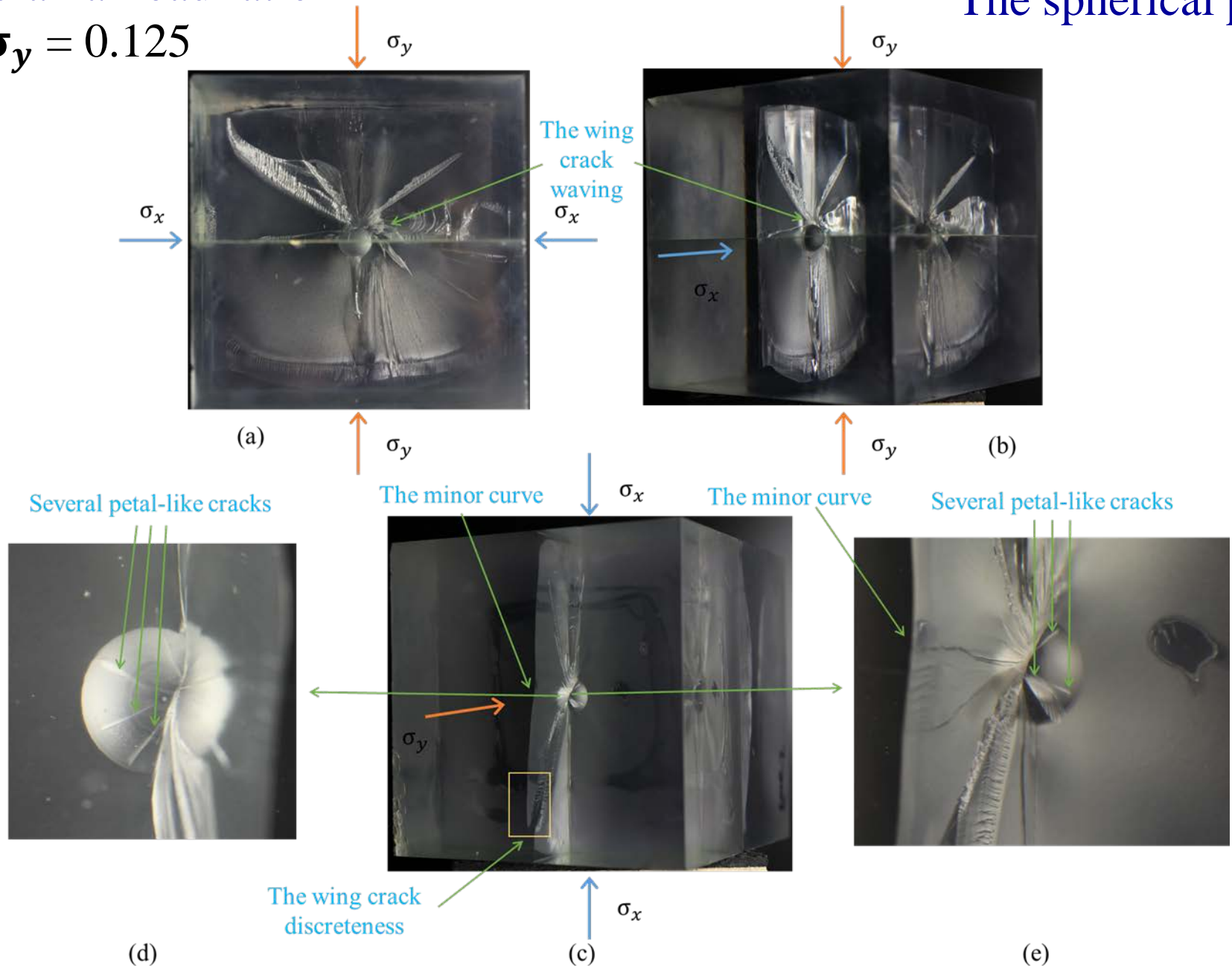
$$\sigma_x / \sigma_y = 0.5$$



# The biaxial load ratio

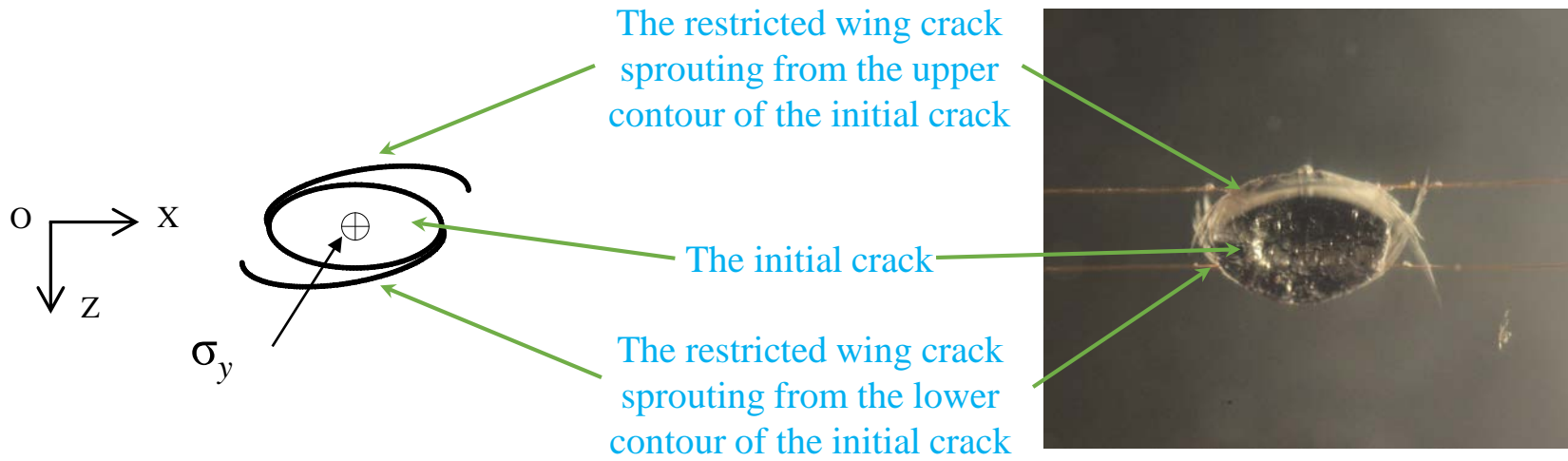
$$\sigma_x / \sigma_y = 0.125$$

# The spherical pore



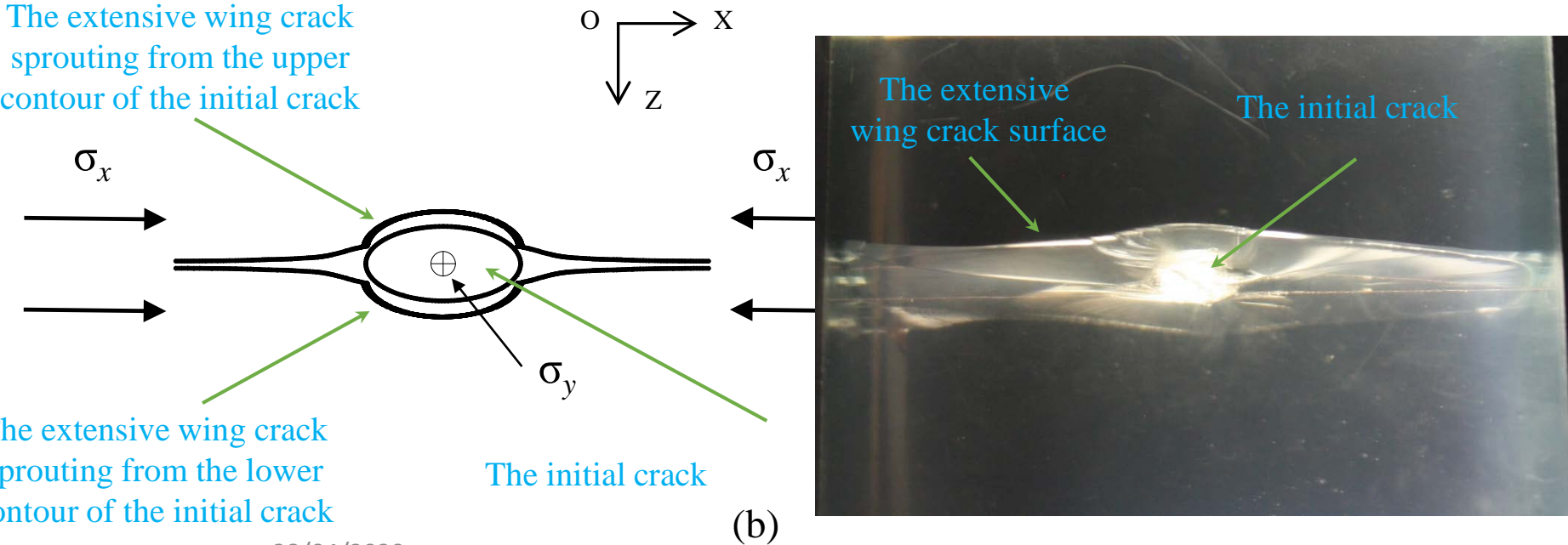
# The experimental results

- Unlike 3-D crack growth in uniaxial compression, which is characterised by the presence of intrinsic limits on 3-D growth of wing cracks associated with wing wrapping, in biaxial compression the wing crack can grow extensively (parallel to a free surface of the specimen) as long as the  $\sigma_x/\sigma_y$  ratio exceeds a threshold. Surprisingly, the threshold is extremely low: around 0.05 for all cases considered; below this threshold, the crack growth is restricted, as illustrated in the following slide.

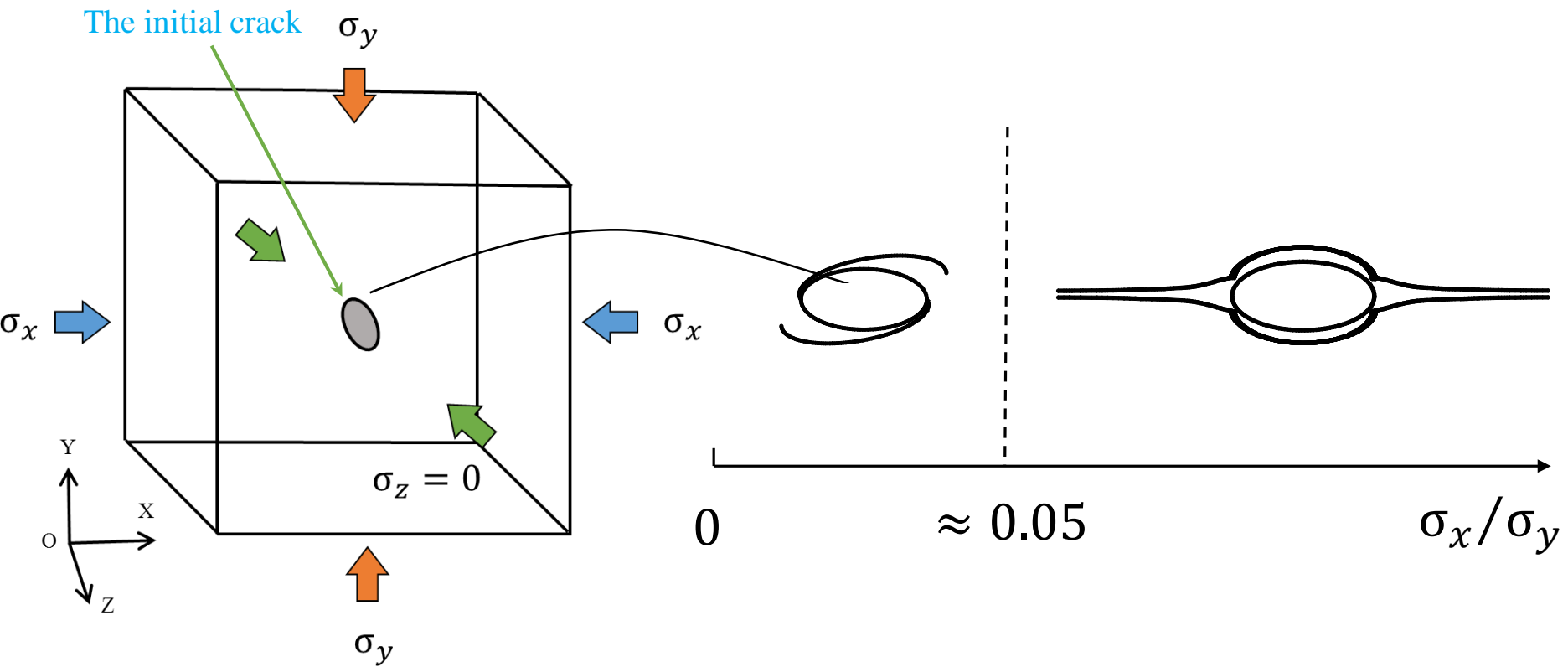


(a)

The extensive wing crack sprouting from the upper contour of the initial crack



(b)

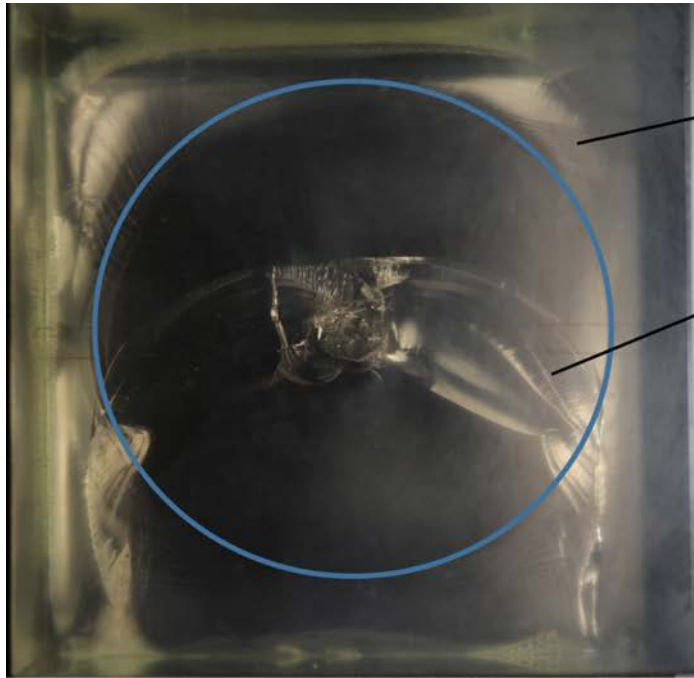


(c)

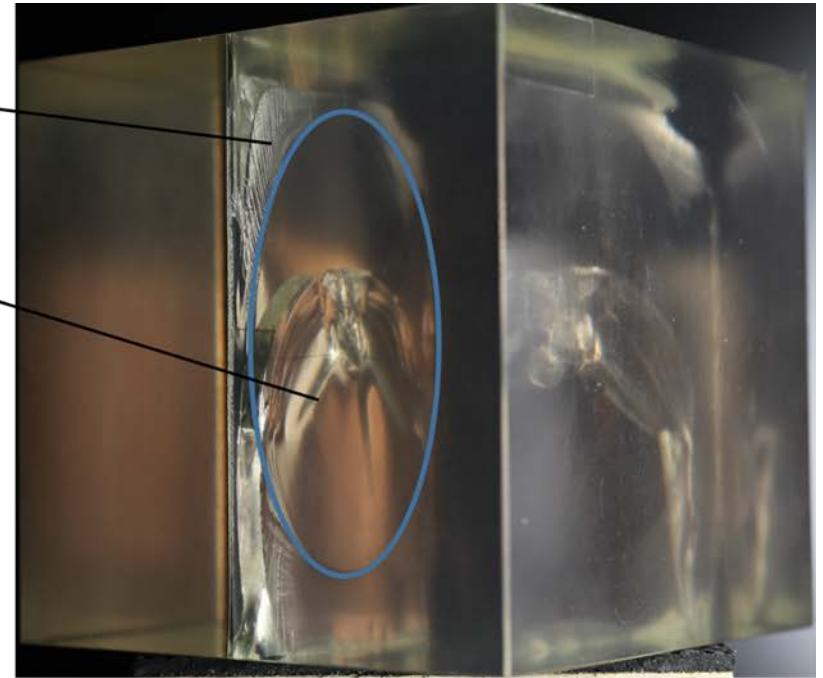
# Two morphologically different regions in a surface of a large wing crack

- The presence of the stable and unstable phases of crack growth can be confirmed by the morphology of the wing crack surface. Two morphologically different regions can be identified during in the surfaces of large wings:
  1. Region I of mirror-like crack surface (the wing crack surface within the blue circle)
  2. Region II of plumose textures in the external part (the part outside the blue circle).
- This transition of crack growing from Region I to Region II is generic, independent on the shape and the orientation of the initial crack, see the experimental results in previous slides.

# Two morphologically different regions of a typical wing crack surfaces



(a)



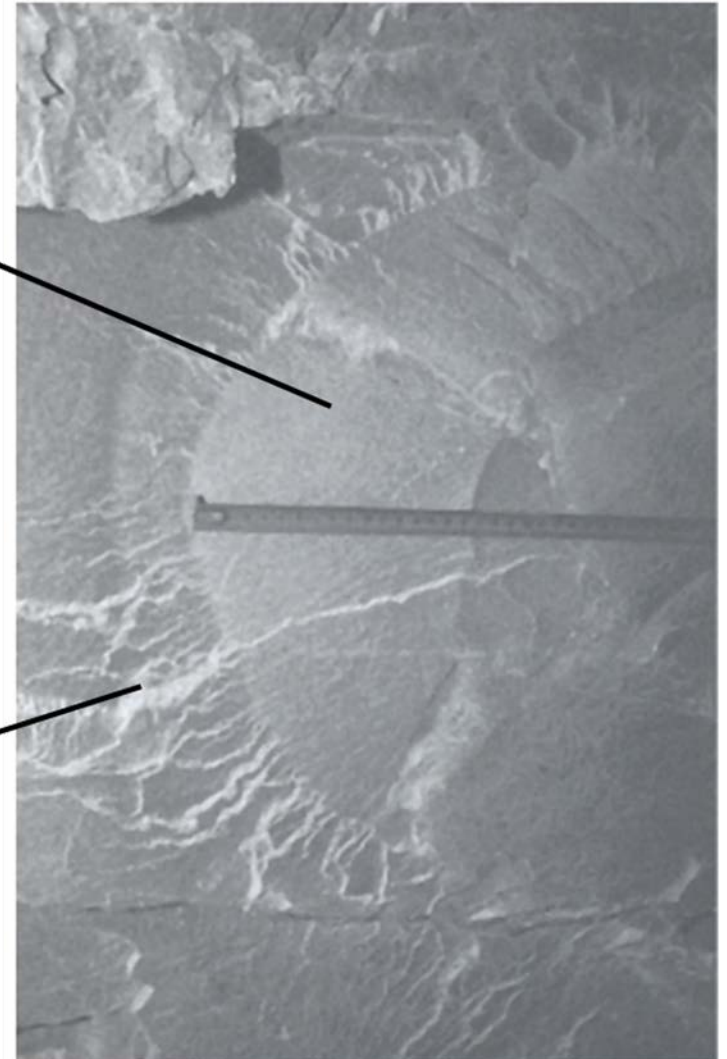
(b)

# The exposed surface of spalling in quartzite sidewall of a Vaal Reefs tunnel

- The presence of these two regions in rock was also detected in the field, demonstrating the exposed surface of a spalling fracture.

Region I

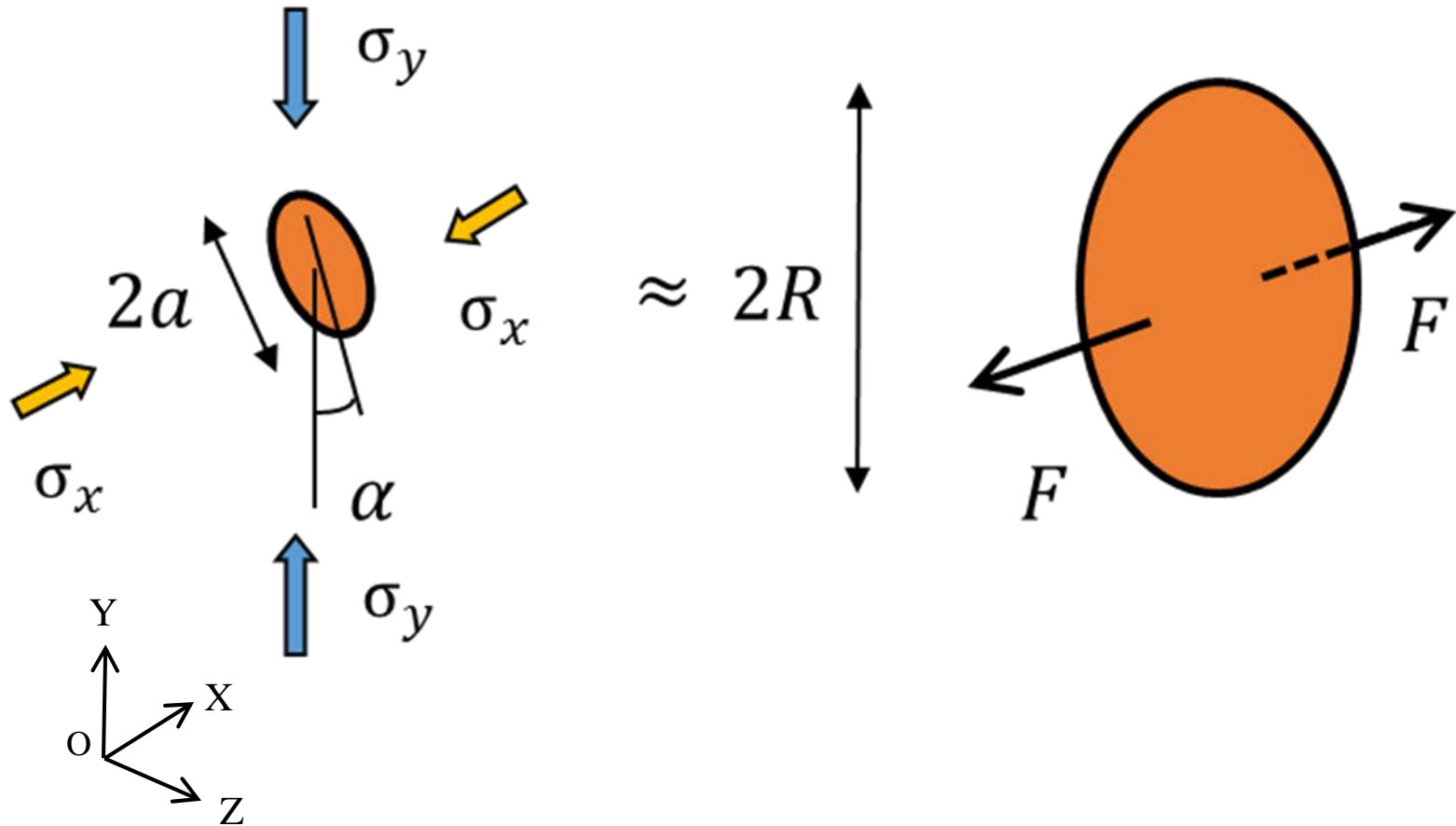
Region II



# Model of 3-D crack growth in biaxial compression

- In order to determine when the stable wing crack growth becomes unstable we use a simplified model. The large growing 3-D wing crack in biaxial compression is modelled as a disc-like crack opened at the centre by a pair of concentrated forces simulating the wedging action of the initial crack, as illustrated in the following slide.
- In the model:  $a$  is the radius of the initial crack,  $\alpha$  is the inclination angle with respect to the plane of the major and intermediate principal stress axes and  $R$  is the radius of the produced wing crack.

# Model of 3-D crack growth in biaxial compression



# Stable phase of crack growth

- Stress  $\sigma_y$  leads to sliding of the opposite faces of a pre-existing crack. This sliding is the same as sliding due to the application of shear stress, Equation (1).
- Neglecting, for the sake of simplicity, friction between the faces of the initial crack and assuming it being penny-shape, the horizontal projection of the total force associated with shear stress  $\tau$  is expressed by Equation (2).
- This concentrated force applied to the disk-like crack of radius  $R$  to simulate the wedging action of sliding over the pre-existing crack. This produces a stress singularity at the contour of the disc-like crack which is characterised by the stress intensity factor, Equation (3).
- The condition of growth of a Mode I crack is formulated in terms of Irwin criterion, Equation (4).

# Stable crack growth

$$\tau = \sigma_y \cos \alpha \sin \alpha \quad (1)$$

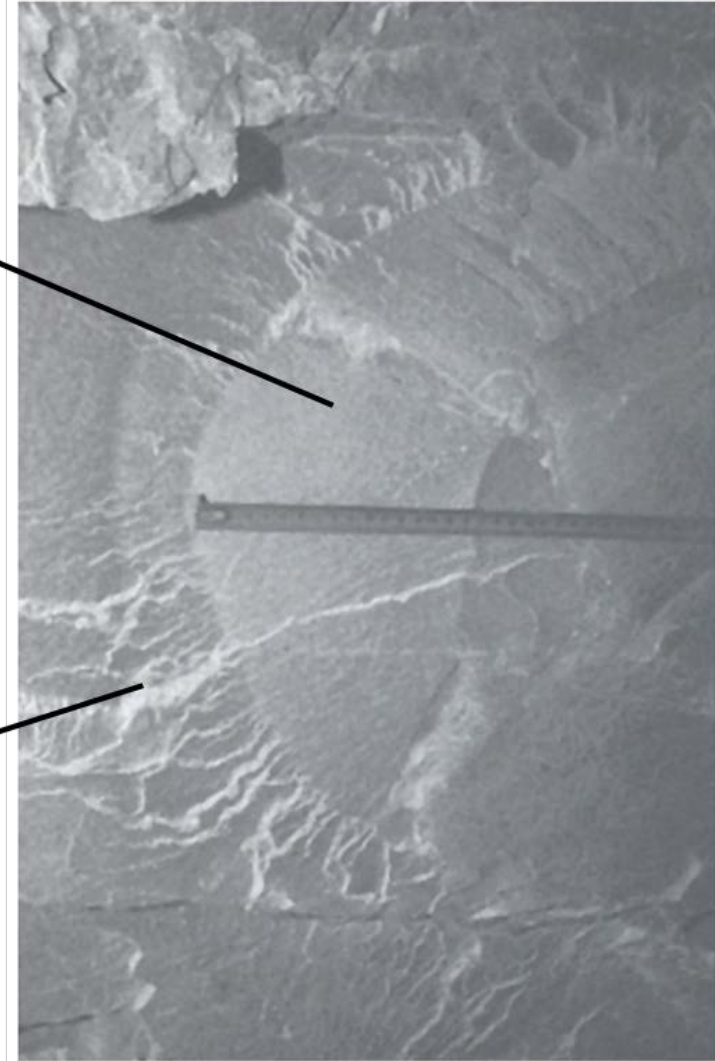
$$F = \pi a^2 \sigma_y \cos \alpha \sin^2 \alpha \quad (2)$$

$$K_I = F(\pi R)^{-3/2} \quad (3)$$

$$K_I = K_{Ic} \quad (4)$$

Region I

Region II



# Onset of unstable phase of crack growth

- Due to interaction with the free planar surface with the increase of the wing crack size, the unstable crack growth will eventually be induced.
- Using the asymptotic solution of Srivastava and Singh for a crack in half-space situated parallel to the free boundary at a distance  $h$  from it, and retaining the main asymptotic term expression, the Model I stress intensity factor can be obtained, Equation (5).
- After normalisation we obtain the following dimensionless expression, Equation (6), where  $r=R/h$ .

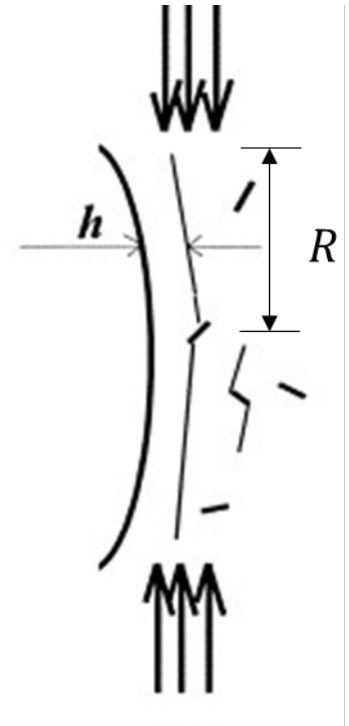
# Onset of unstable crack growth

$$K_I(R) = \frac{F}{(\pi R)^{3/2}} \left[ 1 + \frac{5}{\pi} \left( \frac{R}{h} \right)^3 \right] \quad (5)$$

$h$  is the distance between the wing crack and the free surface

$$K_I h^{3/2} F^{-1} = \pi^{-3/2} \left( \frac{1}{r^{3/2}} + \frac{5}{\pi} r^{3/2} \right) \quad (6)$$

$$r = R/h$$

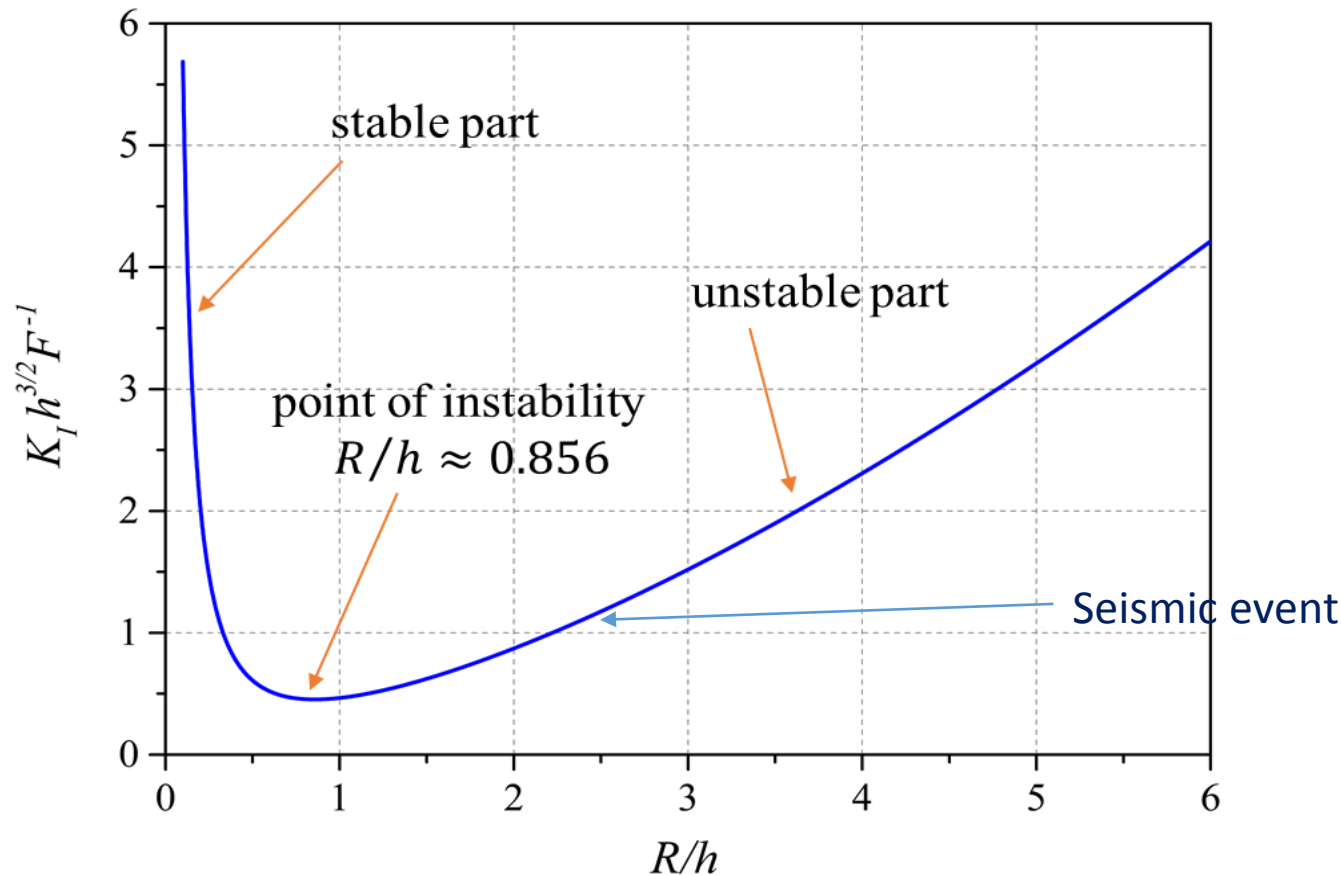


# Unstable phase of crack growth

- The dependence of  $K_I h^{3/2} F^{-1}$  (left part of Equation (6)) on  $R/h$  is plotted in the following figure.
- In this figure, the onset of the unstable regime of crack growth corresponds to the minimum of  $K_I(R)$  by the condition  $dK_I/dR = 0$ . This gives the point (radius) of instability:  $R_c/h = (\pi/5)^{1/3} \approx 0.856$ .
- After this point the stress intensity factor increases with the increase of the wing crack radius leading to a rapid (dynamic) crack growth.

# Unstable phase of crack growth

Normalised stress intensity factor  $K_I$  at the contour of a wing crack interacting with the free surface,  $h$  is the distance to the free surface



The crack is tensile (Mode I) crack, hence the seismic event is the Compensated Linear Vector Dipole (CLVD) source

# Conclusion

- In real, 3-D world, wing crack growth is controlled by intermediate principal stress.
- The critical biaxial load ratios  $\sigma_x/\sigma_y$  inducing extensive crack growth of around 0.05 were found for different types of initial 3-D cracks.
- Extensive crack growth parallel to free face can be induced in biaxial compression.
- The interaction turns an initially stable growth of a crack closest to the free surface into unstable (catastrophic).
- Catastrophic crack propagation produces seismic event: Compensated Linear Vector Dipole (CLVD) source.

# References

Dyskin AV, Sahouryeh E, Jewell RJ, Joer H, Ustinov KB, 2003. Influence of shape and locations of initial 3-D cracks on their growth in uniaxial compression. *Engineering Fracture Mechanics*. 70:2115-36.

Sahouryeh E, Dyskin AV, Germanovich LN. Crack growth under biaxial compression. *Engineering Fracture Mechanics*. 2002,69(18): 2187-2198.

Srivastava KN, Singh K. The effect of penny-shaped crack on the distribution of stress in a semi-infinite solid. *International Journal of Engineering Science*. 1969;7(5): 469-490.

Wang HY, Dyskin A, Pasternak E, Dight P, Sarmadivaleh M. Effect of the intermediate principal stress on 3-D crack growth. *Engineering Fracture Mechanics*. 2018;204:404-20.

Wang HY, Dyskin AV, Pasternak E, Dight P, Sarmadivaleh M. Experimental and numerical study into 3-D crack growth from a spherical pore in biaxial compression *Rock Mechanics and Rock Engineering* 2019 <https://doi.org/10.1007/s00603-019-01899-1>.

Wang HY, Dyskin A, Pasternak E, Dight P. 3D crack growth in biaxial compression: influence of shape and inclination of initial cracks. *Rock Mechanics and Rock Engineering*. 2020.

# Acknowledgements

- AVD and EP acknowledge support from the Australian Research Council through project DP190103260. The first author acknowledges financial support from the Australian Centre for Geomechanics. The authors are grateful to Mr. Frank EE How Tan for his assistance with specimen preparation. AVD acknowledges the support from the School of Civil and Transportation, Faculty of Engineering, Beijing University of Civil Engineering and Architecture.